ACS APPLIED MATERIALS & INTERFACES

Research Article

www.acsami.org

Anhydrous Proton Conducting Polymer Electrolyte Membranes via Polymerization-Induced Microphase Separation

Sujay A. Chopade,[†] Soonyong So,[†] Marc A. Hillmyer,*[,‡] and Timothy P. Lodge*[,‡,†]

[†]Department of Chemical Engineering and Materials Science and [‡]Department of Chemistry, University of Minnesota, Minneapolis, Minnesota 55455-0431, United States

Supporting Information

ABSTRACT: Solid-state polymer electrolyte membranes (PEMs) exhibiting high ionic conductivity coupled with mechanical robustness and high thermal stability are vital for the design of next-generation lithium-ion batteries and high-temperature fuel cells. We present the in situ preparation of nanostructured PEMs incorporating a protic ionic liquid (IL) into one of the domains of a microphase-separated block copolymer created via polymerization-induced microphase separation. This facile, one-pot synthetic strategy transforms a homogeneous liquid precursor consisting of a poly(ethylene oxide) (PEO) macro-chain-transfer agent, styrene and divinylbenzene monomers, and protic IL into a robust and transparent monolith. The resulting PEMs exhibit a bicontinuous morphology comprising PEO/protic IL conducting pathways and highly cross-linked polystyrene (PS) domains. The cross-linked PS mechanical scaffold imparts thermal and mechanical stability to the PEMs, with an elastic modulus approaching 10 MPa at 180 °C, without sacrificing the ionic conductivity of the system. Crucially, the long-range continuity of the PEO/protic IL conducting nanochannels results in an outstanding ionic conductivity of 14 mS/cm at 180 °C. We posit that proton conduction in the protic IL occurs via the vehicular mechanism and the PEMs exhibit an average proton transference number of 0.7. This approach is very promising for the development of high-temperature, robust PEMs with excellent proton conductivities.

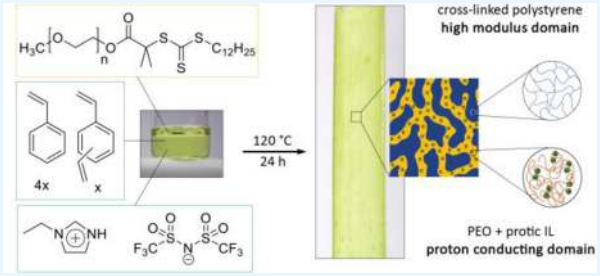

KEYWORDS: *polymer electrolyte membranes, protic ionic liquids, polymerization-induced microphase separation, bicontinuous morphology and high-temperature fuel cells*

INTRODUCTION

Polymer electrolyte membranes (PEMs) that facilitate efficient transport of charged species are critical components of various electrochemical devices.[1−10] Nanostructured PEMs exhibiting distinct structural and ion-conducting phases can offer high ionic conductivity while simultaneously satisfying orthogonal mechanical and/or thermal property requirements (e.g., mechanical robustness, long-term creep resistance, or high-temperature stability).[11,12] One attractive route to such hybrid materials with optimized orthogonal properties involves self-assembled block polymer/ionic liquid (IL) mixtures.[13−22] In such systems, one of the domains selectively incorporates ILs and facilitates ion-conducting pathways, while the other domain, typically glassy and insulating, serves as a mechanical framework providing strength and durability.

ILs are molten salts with low melting temperatures (below 100 °C)[23] and have received significant attention owing to their unique combination of high ionic conductivity, excellent chemical and thermal stability, negligible vapor pressure, and wide electrochemical windows.[24−26] Proton-conducting or protic ILs synthesized using Brönsted acid−base pairs exhibit excellent proton conductivity (≈25 mS/cm at 120 °C) under dehumidified conditions and can be thermally stable even at temperatures in excess of 300 °C.[6,27−29] Accordingly, PEMs incorporating protic ILs are interesting candidates for fuel cells operating at elevated temperatures (100−200 °C) and low humidity. These conditions favor enhanced electrode reaction kinetics and higher tolerance of typical catalysts to carbon monoxide impurities in the hydrogen fuel.[9,10,30−34] Extensive studies on protic ILs and ionic melts consisting of imidazole (Im) and *N*,*N*-bis(trifluoromethylsulfonyl)imide demonstrated that the base-rich IL conducts protons via two mechanisms: vehicular transport of the protonated imidazolium cation (HIm^+) and a faster proton-hopping or Grotthuss-type mechanism involving proton shuttling between HIm^+ and neutral Im molecules.[20,28,29] However, the presence of neutral Im molecules limits the thermal stability of this system.[28,31]

The ionic conductivity of a PEM incorporating an IL is governed by the effective concentration of free ions, the mobility of the ions (strongly dependent on the temperature and flexibility of the polymer), and the connectivity of the conducting pathways.[14,22,35,36] As observed in conventional humidified Nafion membranes, strong segregation between the structural and conducting domains enhances the PEM conductivity.[37] Likewise, in the case of block polymer/IL systems, the IL selectivity for one of the domains could

Received: December 17, 2015
Accepted: February 17, 2016
Published: February 29, 2016

DOI: 10.1021/acsami.5b12366
ACS Appl. Mater. Interfaces 2016, 8, 6200−6210

effectively enhance the conductivity.[22,38] Another structural factor imperative for high conductivity is the presence of well-connected conducting channels spanning the membrane. In a recent study, long-range proton-conducting pathways in sulfonated poly(ether ether ketone) (SPEEK) membranes enriched with IL using functionalized graphene oxides significantly enhanced the membrane conductivity in comparison to a SPEEK control.[39] In contrast, block polymer/IL membranes, designed by solvent casting a mixture of polymer and IL, frequently develop network defects such as grain boundaries, dead ends, and isolated domains that disrupt the continuity of the conducting channels.[19,40] For example, block polymer PEMs with lamellar or conducting cylindrical domains essentially require the conducting pathways to be perpendicularly oriented to the electrode surface for optimal performance.[36] Grain alignment induced by shearing[41] or magnetic or electric fields[41] has been used to increase the conductivity of lamellar samples. On the other hand, isotropic, bicontinuous morphologies (e.g., double gyroid) featuring three-dimensional ion-transport pathways do not require domain alignment. However, the gyroid phase occurs over a relatively narrow range of block volume fractions and is often difficult to access experimentally.[42] In all cases, PEMs prepared with diblock copolymers are expected to be mechanically very weak.

The desired robustness, superior thermal stability, and high ionic conductivity in IL-containing block polymer membranes can be accomplished by designing the PEM with a bicontinuous morphology consisting of a cross-linked mechanical scaffold intertwined with continuous IL-rich conducting nanochannels.[33,43−45] In this work, we developed a proton-conducting PEM using a simple yet versatile one-pot synthetic strategy involving a recently developed polymerization-induced microphase separation (PIMS) method.[43] Bulk copolymerization of monofunctional and difunctional monomers in the presence of a macro-chain-transfer agent (macro-CTA) mixed with IL leads to in situ cross-linking that kinetically traps a disordered network structure adopted by the growing diblocks, thereby imparting a cocontinuous network morphology to the resulting PEM.[46,47] Specifically, reversible addition−fragmentation chain-transfer (RAFT) polymerization was implemented for the controlled growth of styrene (S) and divinylbenzene (DVB) from a poly(ethylene oxide) macro-chain-transfer agent (PEO-CTA) in the presence of a stoichiometric protic IL, 1-ethylimidazolium bis(trifluoromethylsulfonyl)imide, [HEIm][TFSI] (Scheme 1). PIMS allows the direct incorporation of the protic IL into the bicontinuous PEM matrix, yielding isotropic proton-conducting pathways of PEO and IL, along with a cross-linked PS network that imparted mechanical integrity and thermal stability to the system. The morphology, ionic conductivity, and proton-transport characteristics of PIMS PEMs were explored. We concluded that the IL selectivity and increased effective segregation between the mechanical phase and conducting domain enhance the overall conductivity. The PIMS PEMs exhibit long-range, isotropic, continuous-conducting, cross-linked domains with an exceptional combination of ionic conductivity, thermal stability, and mechanical robustness, making them promising candidates for high-temperature proton-transport applications.

EXPERIMENTAL SECTION

Synthesis of the PEO-CTA and IL. Poly(ethylene glycol) methyl ether (M_n = 5 kg/mol; $Đ$ = 1.1) was purchased from Sigma-Aldrich. The RAFT agent *S*-dodecyl-*S*′-(α,α′-dimethyl-α″-acetic acid)-trithiocarbonate (DDMAT) was synthesized as previously reported.[48] The macromolecular PEO-CTA was synthesized by end functionalization at the hydroxyl terminus of the polymer with DDMAT via an acid chloride intermediate. Complete end functionalization was confirmed by ^{1}H NMR end-group analysis (Figure S1) and through the controlled growth of linear PEO-*b*-PS (Figure S2). The IL was prepared by the neutralization of as-purchased (Sigma-Aldrich) 1-ethylimidazole (EIm; ≥95%) with *N*,*N*-bis(trifluoromethylsulfonyl)-imide (HTFSI; ≥95%). An equimolar mixture of EIm and HTFSI was heated at 100 °C for 2−3 h. Activated charcoal (10 wt %) was added to the IL, and the mixture was stirred for 24 h to remove impurities. Dichloromethane was then added, and the mixture was filtered. The IL was dried at 70 °C under dynamic vacuum for at least 2 days and then transferred to an argon atmosphere glovebox. The measured melting point of the IL (−12 °C) agreed well with a previously reported value.[9]

Scheme 1. Reaction Scheme Used To Synthesize a Cross-Linked PEM from 5 kg/mol PEO-CTA and a Protic IL [HEIm][TFSI], Styrene/Divinylbenzene Monomer Mixture

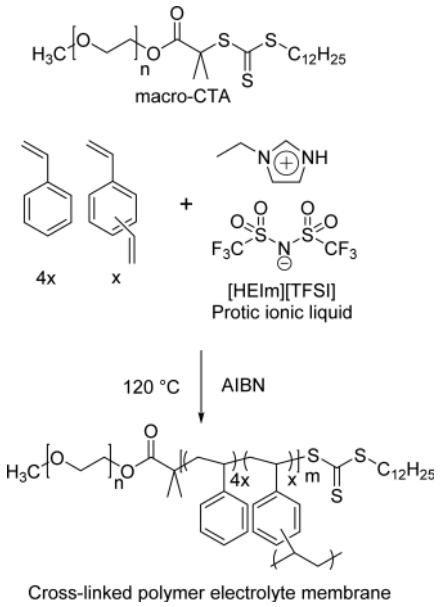

Preparation of PEMs. To develop nanostructured PEMs, reaction mixtures were prepared gravimetrically, typically containing 32 wt % PEO-CTA in a 4:1 molar mixture of styrene to divinylbenzene. A varying amount of the IL was added to this reaction solution to achieve an overall 5−55 wt % IL concentration in the resulting PEM (Table 1). Styrene (S; 99%, Sigma-Aldrich) and divinylbenzene (DVB; technical grade 80%, Sigma-Aldrich) were filtered through an activated alumina column prior to use. The liquid reaction precursor was prepared in glass vials by adding a predetermined amount of the IL to

Table 1. Composition of the PEM Samples

sample name	IL (overall wt %)	composition (vol %)[a]		
		IL	PEO + IL[b]	IL in the PEO + IL domain[c]
PIMS-55	55	45	61	74
PIMS-45	45	35	54	65
PIMS-35	35	27	48	56
PIMS-25	25	18	42	43
PIMS-15	15	10	36	28

[a]The composition was calculated based on the following densities (g/cm^3): $\rho_{PS/DVB}$ = 1.05, ρ_{PEO} = 1.06, and $\rho_{HEIm/TFSI}$ = 1.43. [b]Volume content of the conducting phase. [c]Volume content of the IL in the conducting phase.

DOI: 10.1021/acsami.5b12366
ACS Appl. Mater. Interfaces 2016, 8, 6200−6210

the PEO-CTA inside a glovebox. The monomers (S and DVB) and 2,2′-azobis(isobutyronitrile) initiator (0.05 equiv relative to the PEO-CTA) were injected through a rubber septum into the glass vials containing the IL + PEO-CTA mixture outside the glovebox. The entire solution was stirred and then heated in sealed glass vials at 120 °C for 24 h (Scheme 1). The resulting transparent yellow solid monolith was obtained by breaking the glass vial (Figure S3).

Small-Angle X-ray Scattering (SAXS). SAXS measurements were performed at the Advanced Photon Source (APS) at Argonne National Laboratory using beamlines 5-ID-D and 12-ID-B. The measurements were performed at room temperature using X-rays with a wavelength (λ) of 0.76 Å, yielding scattering wavevectors q [$q = 4\pi \sin(\theta/2)/\lambda$, where θ is the scattering angle] in the range of 0.022−1.35 nm^{-1}. The SAXS intensity as a function of q was obtained by azimuthally integrating the isotropic two-dimensional (2D) scattering patterns.

Scanning Electron Microscopy (SEM). PEO and IL domains of the PEM were etched to create contrast for direct observation of the morphology via SEM. Following an established etching procedure,[49] chunks of the PEM monolith were immersed in an aqueous solution of 57 wt % hydroiodic acid at 60 °C for 5 days, removed and rinsed in methanol, and dried in an oven for 30 h. The etching procedure resulted in >95% removal of the PEO and IL by gravimetric analysis. The freeze-fractured surface of the SEM sample was sputter-coated with ∼1−2 nm of platinum and was imaged using a Hitachi S-4700 high-resolution field-emission-gun scanning electron microscope at an accelerating voltage of 5 kV.

Impedance Spectroscopy. The ionic conductivity of the PEM samples was measured by two-point probe impedance spectroscopy using a Solartron 1255B frequency response analyzer and an SI 1287 electrochemical interface. Samples for conductivity measurements were prepared by sanding bulk PEM monoliths to uniform thickness (ca. 0.5 mm; Figure S3) and stored in an argon-filled glovebox. Prior to the conductivity measurements, the thin samples were dried overnight at 80 °C under dynamic vacuum, then sandwiched between polished stainless steel electrodes, and inserted into a custom-built heating stage. The heating stage and sample were kept in a desiccator to maintain a dry environment. The impedance was measured by applying an alternating voltage with an amplitude of 100 mV over the frequency range of $1-10^6$ Hz. The ionic conductivity, σ, was calculated as t/Ra, where t and a are the thickness and superficial area of the sample and R is the bulk resistance. The bulk resistance was determined from the frequency-independent plateau of the real component of the impedance (Z'; representative raw impedance data are shown in Figure S8). The measurements were performed starting from 180 °C and cooling to 40 °C in 10 °C decrements. At each temperature, the samples were maintained for at least 1 h to allow for thermal equilibration before measurements. Replicate conductivity experiments were performed for both heating (from 40 to 180 °C) and cooling (from 180 to 40 °C) cycles to determine whether any water absorption affected the conductivity of the PEMs. The replicate measurements confirmed the thermal reversibility for the PEM samples (Figure S5). The ionic conductivities of the IL and a PEO homopolymer + IL mixture were measured using a custom-built conductivity cell, which was maintained under a positive argon atmosphere. In this case, σ was calculated as κ/R, where R is the bulk resistance and κ is the cell constant for the conductivity cell, which was calibrated using a 0.01 M KCl standard (Fluka, 1.413 mS/cm at 25 °C).[46]

Diffusion Coefficient Measurements. A Bruker Avance III 500 MHz NMR spectrometer equipped with a 5 mm triple-resonance broad-band pulsed-field-gradient (PFG) probe was used to determine the self-diffusion coefficients of $HEIm^+$ and $TFSI^-$ ions confined inside the PEM. The PEM samples were ground into fine powders and loaded into NMR tubes along with dodecane-d_{26}, a poor solvent for the IL. For the PFG-NMR experiments, the "ledbpgp2s" pulse sequence (longitudinal eddy current delay experiment using bipolar gradients acquired in 2D)[50] was used with two different nuclei, ^1H for $HEIm^+$ and ^{19}F for $TFSI^-$, at different temperatures from 298 to 348 K. At each temperature, the sample was equilibrated for at least 30 min before the NMR experiment was conducted. The translational diffusion coefficients were obtained by using eq 1

$$\frac{I}{I_0} = \exp[-\gamma^2\delta^2G^2D(\Delta - \delta/3)] \quad (1)$$

where I/I_0 is the attenuated intensity (I) at various gradient strengths (G) from 2 to 98% of the maximum G (0.47 T/m) normalized to I_0 at $G = 0$ and γ is the gyromagnetic ratio. The γ values of ^1H and ^{19}F were 42.6 and 40.1 MHz/T, respectively. The diffusion time (Δ) was 100 or 150 ms, and the gradient pulse time (δ) was 4 or 2 ms for both nuclei. The PFG-NMR results were processed by the *TopSpin* software package (version 3.1) and fitted with eq 1.

Mechanical Properties. Tensile-bar-shaped PEM samples were synthesized by reacting the liquid precursor in Teflon molds at 120 °C. The mechanical response of these tensile bars, measuring approximately 50 × 10 × 0.8 mm^3, was analyzed using a TA Instruments RSA-G2 solid analyzer. The linear viscoelastic regime was determined by strain sweeps performed at a frequency of 10 rad/s at various temperatures. Frequency sweep experiments were performed at a fixed strain amplitude over the frequency range of 1−100 rad/s for the temperature range of 30−210 °C under a nitrogen atmosphere; the sample was equilibrated at a given temperature for at least 10 min. A time-temperature superposition (tTS) master curve was developed by horizontally shifting and aligning the frequency sweep data for the elastic modulus, E'.

Thermal Properties. Differential scanning calorimetry (DSC) measurements were carried out using a TA Instruments Discovery differential scanning calorimeter. Samples prepared using aluminum T-zero pans with hermetic lids were annealed at 180 °C for 10 min, followed by subsequent cooling and heating ramps at 10 °C/min. Thermogravimetric analysis (TGA) of the PEM samples was performed on a TA Instruments Q500 under a nitrogen atmosphere at a heating rate of 10 °C/min from room temperature to 450 °C. The PEM samples were dried at 50 °C under dynamic vacuum overnight prior to the measurements.

RESULTS

Characterization of the PEM Morphology. This synthesis strategy enables PEM preparation over a wide IL composition range (5−55 overall wt % [HEIm][TFSI]), thus facilitating optimization in terms of the mechanical properties, ionic conductivity, and morphology. Typical room temperature SAXS profiles, as shown in Figure 1, exhibit a broad principal scattering peak at q^* and a weak higher order shoulder at approximately $2q^*$ in most cases, characteristic of a structured morphology with microphase-separated domains but without long-range periodic order.[51] The position of the primary scattering peak corresponds to the structural length scale of compositional heterogeneities ($d = 2\pi/q^*$). In the PEM samples prepared with [HEIm][TFSI], the characteristic length scale between the PEO/IL and P(S-*co*-DVB) domains is 20−24 nm, significantly higher than the domain spacing between PEO and the cross-linked PS phase (≈12 nm) in samples without ILs.

With increasing IL concentration in the PEM, an increase in the average domain spacing between the conducting phase and the cross-linked PS phase was observed, consistent with selective swelling of the PEO domains by the IL and increasing chain stretching at the (PEO + IL)/P(S-*co*-DVB) interface to reduce the unfavorable interactions.[16,52] The interfacial chain stretching can be ascribed to this selective incorporation of the IL and the resulting increase in the effective interaction parameter, χ_{eff}, between P(S-*co*-DVB) and the conducting phase (PEO + IL), compared to that between P(S-*co*-DVB) and pure PEO.[53] A higher segregation strength also leads to an

DOI: 10.1021/acsami.5b12366
ACS Appl. Mater. Interfaces 2016, 8, 6200−6210

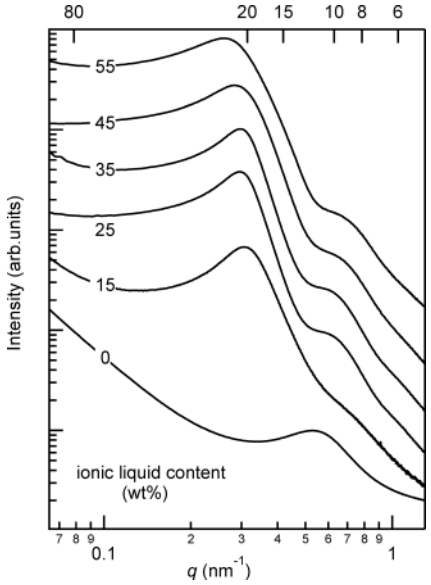

Figure 1. SAXS data for PIMS PEM samples prepared with 5 kg/mol PEO-CTA and variation of the protic IL [HEIm][TFSI] content. The length scale of compositional heterogeneities increases slightly with the IL content (reported as overall wt %).

increased local order, as indicated by the appearance of a more pronounced shoulder at ca. $2q^*$ at higher IL concentrations.

SEM micrographs (Figure 2) of freeze-fractured surfaces of PEMs subjected to PEO/IL etching conditions and coated with a ∼1−2 nm platinum layer show uniformly distributed, interconnected pores, consistent with the formation of a bicontinuous morphology with interpenetrating domains of cross-linked PS and PEO/IL conducting phases. The pores/voids correspond to regions of PEO/IL prior to etching, whereas the bright regions represent the unetched cross-linked PS domains. As expected, the porous volume in the etched samples increases with the IL content (Figure 2b,c). The absence of long-range order is in agreement with the absence of higher-order scattering peaks. The sample-spanning bicontinuous nature of the PIMS PEM morphology was also confirmed by the agreement (within experimental error) between the weight loss during the etching process and the corresponding mass fraction of the PEO + IL phase in the PEM. The SEM images thus corroborate the SAXS results, highlighting the existence of a bicontinuous morphology in the PEM system consisting of microphase-separated domains that lack long-range order.

Ionic Conductivity. The ionic conductivity of PEM samples prepared with overall IL concentrations of 15−45 wt % was measured as a function of temperature (Figure 3). The conductivity of the PEMs increases with both increasing temperature and IL content. Table 1 summarizes the concentrations of all of the species in the various samples and the composition of the PEM in terms of the volume percent of the conducting phase (PEO + IL) and the volume percent of the IL in the overall PEM and in the conducting phase. The conductivity data were fit to the Vogel−Fulcher−Tammann (VFT) relationship

$$\sigma = \sigma_0 \exp\left(\frac{-B}{T - T_0}\right) \quad (2)$$

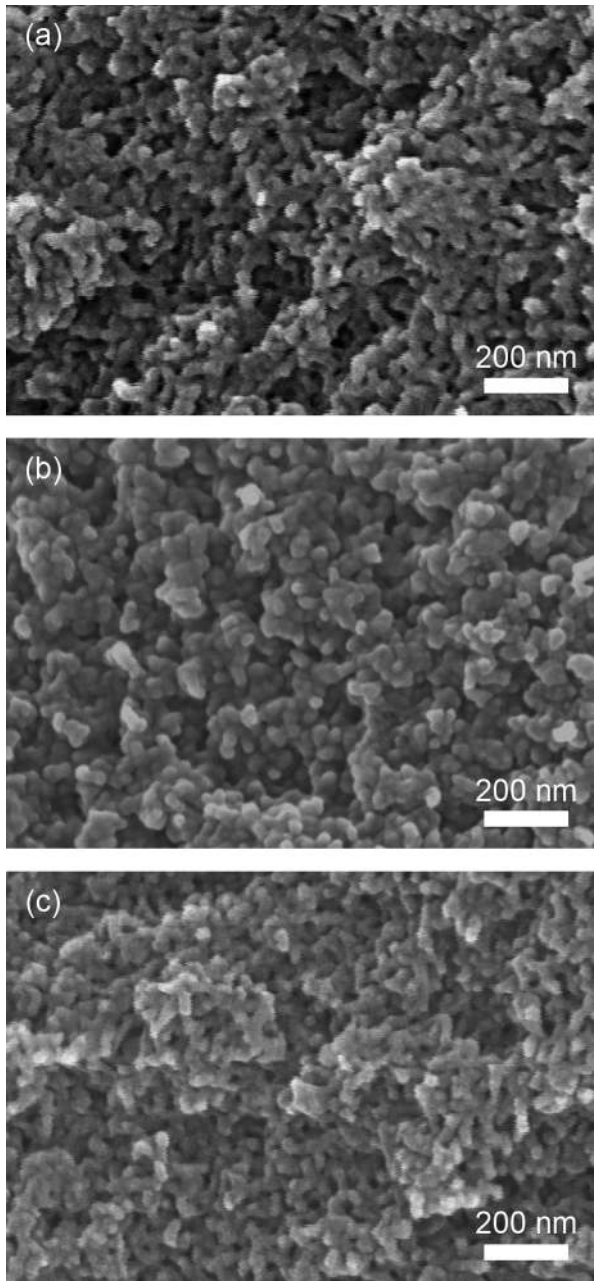

Figure 2. SEMs of the PIMS PEM samples after etching of the PEO domains and the protic IL [HEIm][TFSI]. PEMs with IL contents of (a) 0 wt % (no IL), (b) 35 overall wt %, and (c) 55 overall wt %. Freeze-fractured samples were coated with 1−2 nm of platinum prior to imaging. The bright regions in the micrographs are the unetched PS domains. Uniformly distributed, interconnected pores confirm the bicontinuous morphology.

where the prefactor, σ_0, represents the asymptotic conductivity of the PEM system at infinite temperature, B is a pseudoactivation energy, and T_0 is the Vogel temperature, at which all of the molecular motion is frozen and the conductivity approaches zero.[35] The VFT parameters for these data are given in Table S1.

Figure 3 summarizes the ionic conductivity of PEMs in comparison to the protic IL. The choice of [HEIm][TFSI] as a model protic IL was motivated by its favorable thermal properties (glass transition temperature $T_g \approx -89$ °C;[9] high decomposition temperature $T_d \approx 385$ °C) and high ionic

DOI: 10.1021/acsami.5b12366
ACS Appl. Mater. Interfaces 2016, 8, 6200−6210

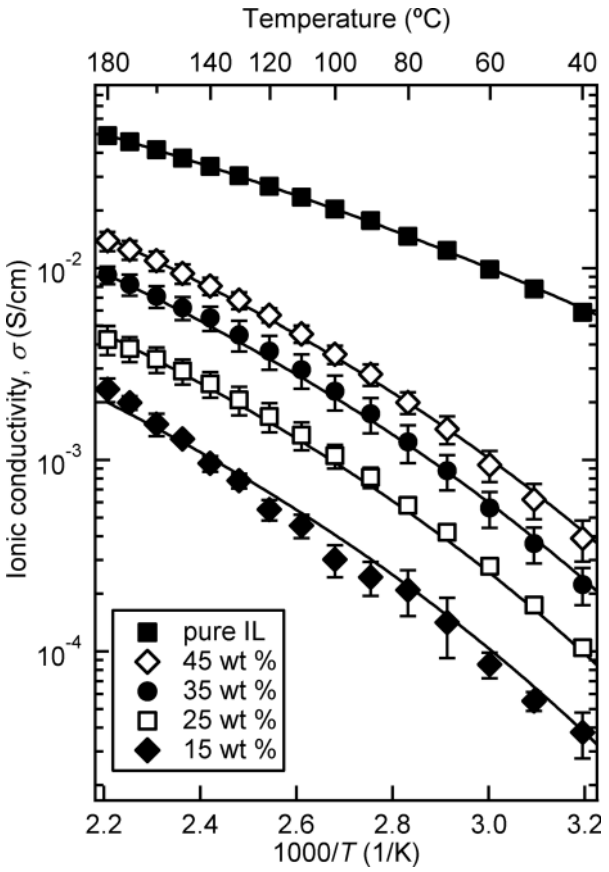

Figure 3. Ionic conductivity of the PIMS PEM samples with varying content of the protic IL [HEIm][TFSI] (reported as overall wt %). Solid lines are fits to the VFT functional form; VFT parameters are provided in Table S1. Error bars (in some cases smaller than the data points) are one standard deviation based on at least three measurements. The IL conductivity (■) of pure [HEIm][TFSI] is also shown for reference.

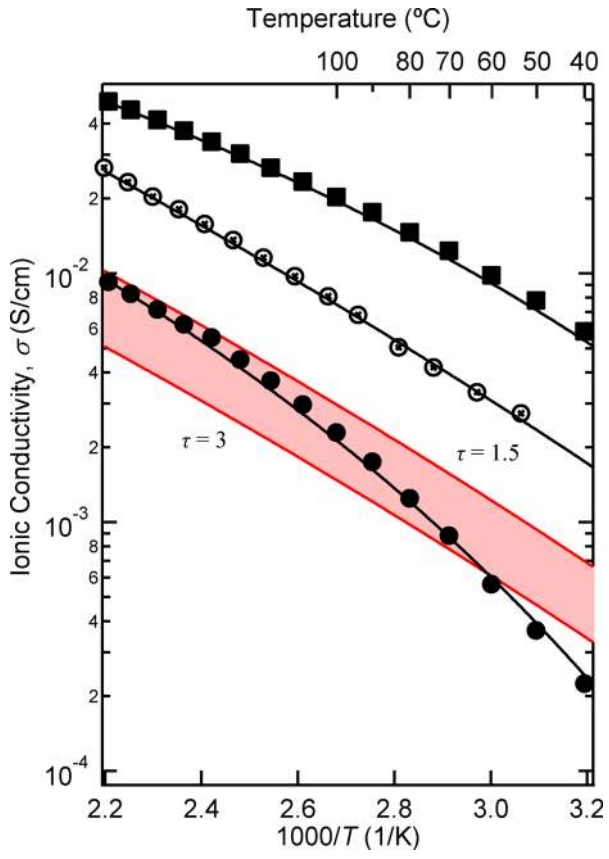

Figure 4. Comparison of the PIMS-35 (35 wt % IL) conductivity (●) to that of the tortuosity model (eq 3). The homogeneous electrolyte (⊗) was prepared with a 5 kg/mol PEO homopolymer/[HEIm][TFSI] mixture with the same composition as the conducting phase (PEO + IL) in PIMS-35 at 56 vol % IL. The red region is defined according to eq 3 with f_c = 0.48 (volume fraction conducting phase in PIMS-35) and $1.5 \leq \tau \leq 3$. The IL conductivity (■) of pure [HEIm][TFSI] is also shown for reference.

conductivity. PIMS-45 (a PEM sample with 45 wt % IL) exhibited an impressive ionic conductivity on the order of 14 mS/cm at 180 °C. It is worth noting that the PIMS PEMs with even lower IL content showed appreciable ionic conductivity, in contrast to some reports in the literature.[10,22] For example, PIMS-15 consists of 10 overall vol % IL, which is lower than the theoretical percolation threshold (≈15 vol %) required to form a sample-spanning network.[54] Nevertheless, this PEM exhibited substantial ionic conductivity (◆ in Figure 3). This result highlights the fact that network defects like dead ends and isolated domains are rare in PIMS PEMs and the PEO + IL phase forms continuous-conducting nanochannels.

To assess the long-range connectivity of the conducting channels as suggested by the SEM images, the conductivity of the PIMS-35 PEM sample was compared to σ_h, the conductivity of a bulk, homogeneous PEO + IL electrolyte (⊗ in Figure 4). In the absence of any network defects and IL dead pockets, the PEM conductivity (σ) can be expressed using a tortuosity model as a fraction of the conductivity of a bulk, homogeneous electrolyte (σ_h) with the same PEO/IL composition as the conducting phase of PEM by

$$\sigma = \sigma_h \frac{f_c}{\tau} \quad (3)$$

where f_c and τ are the volume fraction and tortuosity of the conducting phase (PEO + IL), respectively. In the case of PIMS-35, f_c = 0.48 (Table 1). The tortuosity parameter, τ, accounts for the relatively longer path ions have to travel in comparison to the distance between the electrodes. τ values for molecular transport in a cocontinuous network are expected to be between 1.5 and 3.[55−57] As seen in Figure 4, the measured ionic conductivity of PIMS-35 (●) is generally consistent with eq 3 (represented by the red-shaded region) and the expected range of the tortuosity ($1.5 \leq \tau \leq 3$). This result indicates that the conducting nanochannels are predominantly continuous, with few network defects like dead ends or grain boundaries. The result also highlights that the rigid cross-linked PS phase does not significantly impede the ion transport, implying a relatively narrow interface between the domains.

The ionic conductivity of the PEM is proportional to that of the homogeneous electrolyte at higher temperatures (>100 °C) but drops more quickly at lower temperatures. The tortuosity model ignores the fact that PEO chains in the PEM are tethered to the cross-linked PS domains. At lower temperatures, the close proximity of the glassy PS phase likely slows the relaxation dynamics of the PEO chains in the PEM conducting phase and therefore lowers the overall conductivity. Nevertheless, the long-range connectivity of the conducting

DOI: 10.1021/acsami.5b12366
ACS Appl. Mater. Interfaces 2016, 8, 6200−6210

nanochannels, as corroborated by the tortuosity model, imbues the PIMS PEM with an exceptional ionic conductivity.

Proton-Transport Characteristics. Impedance spectroscopy reflects the contributions of both ions to the overall ionic conductivity of the PEM sample, whereas only the cation contributes to the desired proton conduction. The proton conductivity can be estimated by identifying the proton transference number, t^+, given by

$$t^+ = \frac{D^+}{D^+ + D^-} \tag{4}$$

where D^+ and D^- are the diffusion coefficients of the proton and anionic species, respectively.[10] Owing to the highly acidic nature of HTFSI ($pK_a = -10$),[58] it is reasonable to assume that all EIm species in an IL mixture with stoichiometric amounts of acid and base are in the protonated form.[31] The PFG-NMR experiments with a ^{1}H probe provided the diffusion coefficients of the C−H proton and the exchangeable N−H proton of the $HEIm^+$ cation or the D^+ in the PIMS PEM (Figure S9). In the absence of any free base (i.e., EIm), proton conduction in the stoichiometric protic IL predominantly occurs via a vehicular mechanism governed by transport of the $HEIm^+$ cations.[9,10] In the case of the PIMS-35 sample, the measured diffusion coefficients of the C−H and N−H protons of $HEIm^+$ are almost the same (Figure S10), indicating that proton transport in the PEM basically occurs via the vehicular mechanism. PFG-NMR experiments with a ^{19}F probe provided the diffusion coefficient of the fluorine atoms on the $TFSI^-$ anion, D^-. A typical example of I/I_0 as a function of $\gamma^2\delta^2G^2(\Delta - \delta/3)$ is shown in Figure S11, where the slopes of the plots provide the D^+ and D^- diffusion coefficients. In all of the PFG-NMR experiments, dodecane-d_{26} was added to an NMR tube loaded with a fine powder of PEM to achieve better locking and shimming. Dodecane-d_{26} is a poor solvent for the IL, the cations and anions were therefore trapped inside the conducting phase of the PEM, and the measurements represent the diffusion coefficients of the ionic species in a PEM environment with tortuous conducting pathways (see the analysis in the Supporting Information for details).

D^+, D^-, and the calculated t^+ of PIMS-35 are listed in Table 2. As expected, the cation diffuses more rapidly than the bulky anion at all experimental temperatures.[59] The proton transference number of the PEM is a weak function of the temperature, indicating that the activation energies for diffusion of the cation and anion are similar (Figure S10). In a separate experiment, t^+ of pure [HEIm][TFSI] at 25 °C was calculated to be 0.62. PIMS-35 exhibits an average transference number of about 0.7, which is slightly higher than that of the IL, possibly because of the presence of anionic aggregates in the PEM system.[20,38] The ionic conductivity of PIMS-45 at ∼180 °C is ≈14 mS/cm (◇ in Figure 3). After accounting for t^+ (≈0.7), the highest proton conductivity at ∼180 °C of the samples prepared to date is nearly 10 mS/cm.

Table 2. Proton and Anion Diffusion Coefficients and Transference Number of PIMS-35

temperature (°C)	D^+ (m^2/s) ($\times10^{-11}$)	D^- (m^2/s) ($\times10^{-11}$)	t^+
25	0.8	0.4	0.67
53	2.6	1.0	0.72
75	3.9	1.8	0.68

Figure 5 compares σ of PIMS-35 (○) measured by impedance spectroscopy and σ calculated using diffusion coefficients (■) from PFG-NMR experiments via the Nernst−Einstein equation

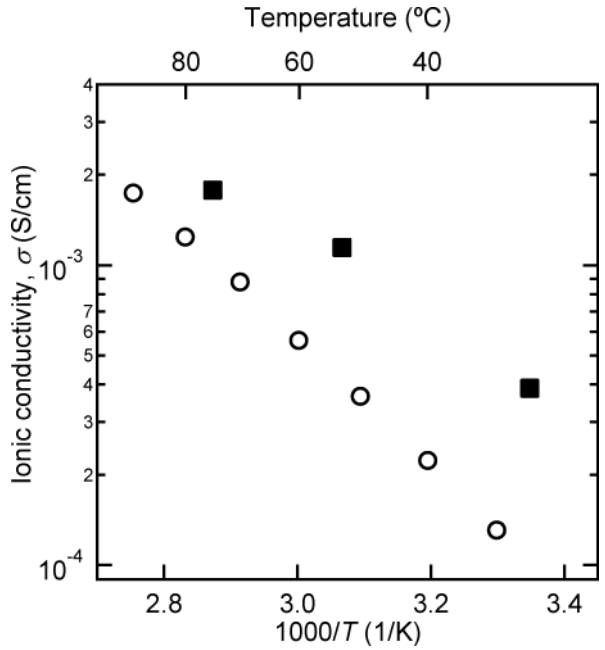

Figure 5. Measured ionic conductivity σ (○) and σ calculated using PFG-NMR diffusion coefficients via the Nernst−Einstein equation (■) of PIMS-35, a PEM with 35 wt % IL overall content.

$$\sigma = \frac{F^2}{RT}(c^+D^+ + c^-D^-) \tag{5}$$

where c^+ and c^- are the molar concentrations of $HEIm^+$ and $TFSI^-$, respectively, F is Faraday's constant, R is the gas constant, and T is the temperature. In the calculation of σ using eq 5, we assume that all of the ionic species are fully dissociated. The Nernst−Einstein equation overpredicts the measured total conductivity of the PEM by a factor of 3−4. The discrepancy is likely attributed to the formation of ion pairs and aggregates with zero effective charge that do not contribute to ion conduction.[38] At lower temperatures, the increased overestimate of the PEM ionic conductivity suggests a higher extent of ionic aggregation in the conducting phase.

Mechanical Properties and Thermal Stability. The highly cross-linked PS mechanical scaffold provides the PIMS PEMs with superior mechanical properties in comparison to analogous block polymer systems incorporating ILs or other salts.[60,61] Figure 6 shows the elastic moduli of the PIMS-35 and PIMS-45 PEM samples (at 10 rad/s frequency) as a function of temperature. Throughout the experimental temperature range (30−210 °C), the PEM samples behave as high-modulus solids. The tensile elastic modulus (E') of the PIMS-35 PEM sample gradually drops from about 110 MPa at 30 °C to about 7 MPa at 210 °C. Further increasing the IL content slightly reduces E'. The tTS master curve (Figure S7), developed by horizontally shifting the raw frequency sweep data, highlights that the mechanical response of the composite PEM is primarily governed by a single phase, the cross-linked P(S-*co*-DVB) network. The mechanical response corroborates the presence of an isotropic sample-spanning continuous PS network. The

DOI: 10.1021/acsami.5b12366
ACS Appl. Mater. Interfaces 2016, 8, 6200−6210

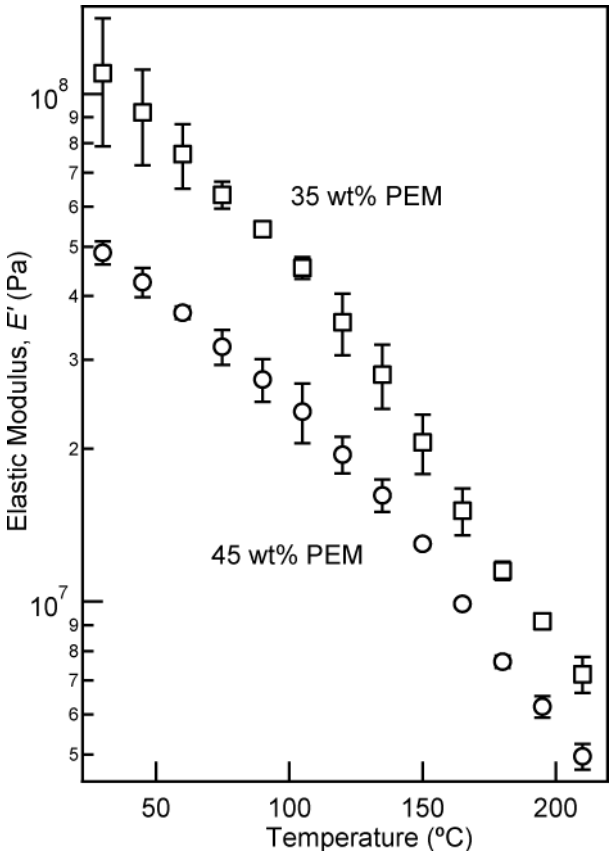

Figure 6. Linear elastic tensile modulus of PIMS-35 and PIMS-45 (PEM samples prepared with 35 and 45 wt % protic IL). The data points represent E' at 10 rad/s and were extracted from isothermal frequency sweeps.

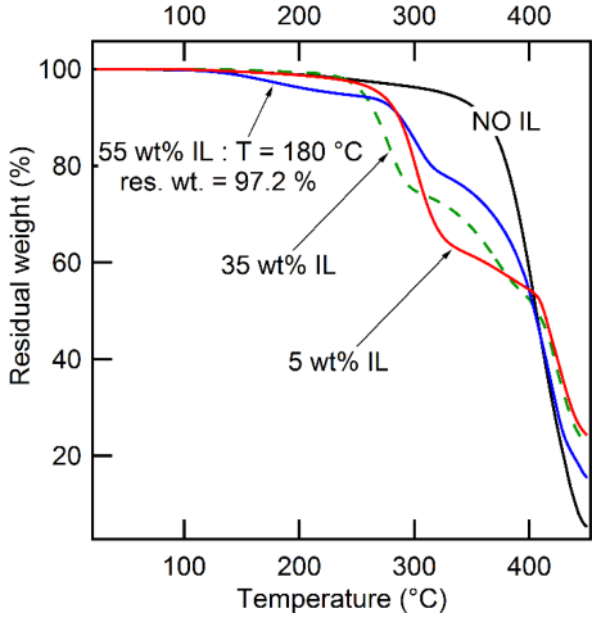

Figure 7. TGA curves under nitrogen of the PIMS PEM samples with varying amounts of protic IL (heating rate: 10 °C/min).

frequency sweeps (Figure S7) do not exhibit any distinct T_g values corresponding to the cross-linked PS phase, consistent with the DSC measurements up to 175 °C (Figure S6).

The thermal stability of the PEM samples was assessed using TGA under a nitrogen atmosphere. As shown in Figure 7, the neat cross-linked PEO-*b*-PS system has excellent thermal stability ($T_d \approx 350$ °C), whereas PEMs are thermally stable up to approximately 270 °C. These PIMS PEMs exhibit thermal stability on par with other high-temperature fuel-cell membranes such as phosphoric acid doped polybenzimidazole membranes.[62] For temperatures above 300 °C, the percent weight loss in PEM samples decreases with increasing IL concentration, highlighting the superior thermal stability of the IL ($T_d \approx 385$ °C)[9] compared to the polymer matrix. In contrast, at temperatures below the T_d values of the PEMs, the thermal stability of the PEM decreases with increasing IL concentration. Similar observations were made during the impedance experiments, where high-IL-content PEMs showed visible degradation when subjected to repeated heating and cooling cycles from 30 to 180 °C. These results can be attributed to the instability of PEO domains in the presence of acidic salts like [HEIm][TFSI][63] (see Table S2).

DISCUSSION

Continuous-Conducting Pathways. The model protic IL [HEIm][TFSI] was selected based on (a) its miscibility with S/DVB monomers to form a homogeneous reaction precursor and (b) the desired incompatibility with PS. PS with $M \geq 3$ kg/mol has been reported to be immiscible with 1-ethyl-3-methylimidazolium bis(trifluoromethylsulfonyl)imide, [EMI][TFSI] (Figure S4), an aprotic IL chemically similar to [HEIm][TFSI].[16,64] Reacting the liquid precursor at 120 °C results in the controlled growth of P(S-*co*-DVB) from PEO-CTA by RAFT polymerization, which leads to partitioning of the IL into microphase-separated domains. Simultaneous growth and cross-linking of the PS block kinetically arrests the system in a cocontinuous morphology that is locally correlated but does not exhibit long-range order.[46,47] During the reaction, IL becomes immiscible with the PS phase and partitions to the PEO-rich regions to form sample-spanning continuous-conducting nanochannels.

In contrast to most block polymer/IL electrolyte systems,[38,65] the PIMS strategy allows the direct incorporation of the IL into conducting nanochannels, thus eliminating postpolymerization steps such as IL doping and domain alignment to achieve appreciable ionic conductivity. The conductivity of self-assembled diblock PEMs is often compromised by grain boundaries and isolated domains.[66] Lee et al. developed PEMs by incorporating a protic IL, diethylmethylammonium trifluoromethanesulfonate into a sulfonated polyimide matrix.[10] The authors observed that PEM with 33 and 55 wt % IL content membranes exhibited low conductivities and a sudden rise in the conductivity of the system for IL contents above 67 wt %. The authors attributed this sudden rise to the establishment of well-connected ion-conducting channels in membranes with IL content higher than 67 wt %. In contrast, these PIMS PEMs exhibited excellent ionic conductivity at IL contents as low as 15 wt %. In addition, the gradual increase in the ionic conductivity with the IL content highlights that sample-spanning continuous-conducting channels are present in the system irrespective of the IL content.

The PIMS PEMs exhibit among the highest ionic conductivities compared to other systems designed using nonionic polymer matrixes and equivalent IL content, such as polystyrene-*b*-poly(2-vinylpyridine) (PS-*b*-P2VP) diblocks in-

DOI: 10.1021/acsami.5b12366
ACS Appl. Mater. Interfaces 2016, 8, 6200−6210

corporating a protic IL, imidazolium bis-(trifluoromethylsulfonyl)imide, [Im][TFSI],[22] and poly-(vinylidene fluoride-*co*-hexafluoropropylene)/IL mixtures.[9] Sulfonated PEMs are fundamentally different from PIMS PEMs because the chemically tethered sulfonic groups along the polymer backbone facilitate proton exchange with the IL and enhance the overall conductivity of the system.[21] In contrast, the PEO domains in the PIMS PEMs appear to be just a "container" for the protic IL, and proton transport in the composite material must be predominantly via the vehicular mechanism.

Sulfonated PEMs in the hydrated form, such as commercial humidified perfluorosulfonic acid polymer membranes like Nafion, have the sulfonate groups affixed to the polymer backbone and therefore have proton transference number $t^+ = 1$. It is worth noting that the PIMS PEMs also exhibit a high proton transference number, on the order 0.7. Furthermore, the anhydrous nature of the PIMS PEMs facilitates proton transport even at elevated temperatures where humidified membranes encounter difficulties. The proton transference number of the PIMS PEMs can further be raised by introducing excess a Brönsted base (EIm), thus increasing the extent of proton transport by the faster proton-hopping or Grotthuss mechanism. However, IL systems with base-rich compositions have relatively poor thermal stability and are therefore less suitable for high-temperature operation. Another issue encountered by PEMs incorporating ILs for fuel-cell applications is the possible leaching of the electrolyte by water, a byproduct of the electrode reactions and resulting in a decrease in the ionic conductivity.[31,67] [HEIm][TFSI], used in the current study, and other ILs with $TFSI^-$ anions are expected to be more stable during a fuel-cell operation because they are relatively more hydrophobic than ILs designed with tetrafluoroborate, BF_4^-, and hexafluorophosphate, PF_6^-, anions.[68] To investigate the IL retention ability of the PIMS PEMs, the membranes were immersed in deionized water. PEMs lose all of the IL after about 5 h (Figure S13).

Segregation Strength and IL Selectivity. To assess the effect of the nature of the IL on the PEM morphology, a comparative study was performed with PEMs incorporating an aprotic IL, [EMI][TFSI] (Figure S4). Key observations made from the comparative SAXS data (Figure 8) are as follows: (i) For the same IL content, the characteristic length scale is larger for the protic IL PEMs. (ii) Protic IL PEMs exhibit more prominent higher-order features. These observations indicate that the effective interaction parameter between the conducting phase and the cross-linked PS phase is larger in the case of the protic IL PEM. Consequently, the more hydrophilic IL [HEIm][TFSI] partitions more strongly into the PEO phase, increasing the interfacial chain stretching to minimize the unfavorable interactions between the IL and the PS phase and thereby yielding a larger average domain spacing.[69]

Similarly, increases in the domain purity and the scattering intensity result in more pronounced higher-order features in the scattering profile. Hoarfrost and Segalman made similar observations about the domain spacing while examining PS-*b*-P2VP diblocks incorporating a protic IL, [HIm][TFSI], and an aprotic IL, [EMI][TFSI].[22] The domain spacing in the PIMS PEM is ultimately determined by the type and concentration of the IL, the molar mass of the polymer blocks, and the extent of cross-linking. In addition to larger domain spacings, the relatively higher degree of segregation in PIMS PEMs with a

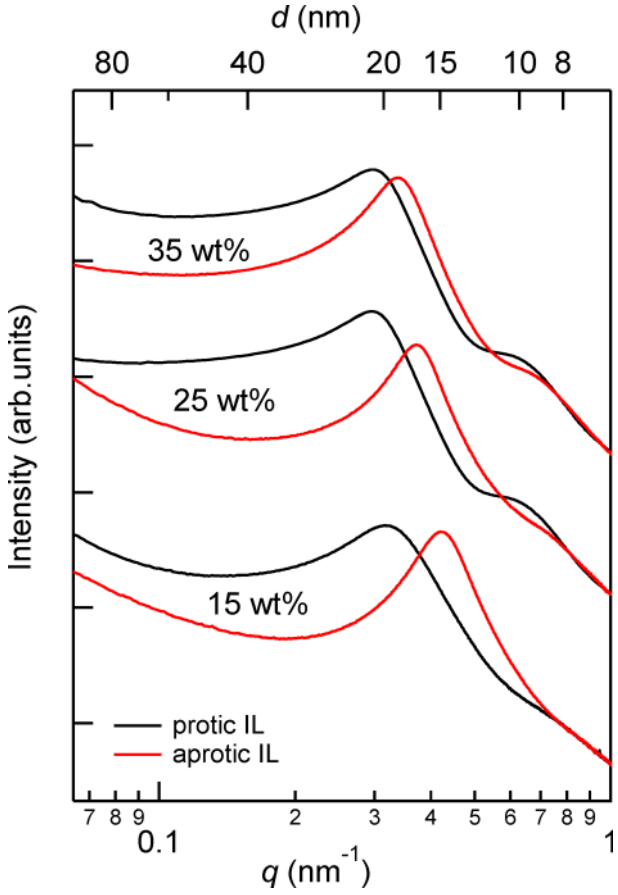

Figure 8. SAXS data for PIMS PEM samples prepared with 5 kg/mol PEO-CTA and varying protic IL [HEIm][TFSI] (black traces) and aprotic IL [EMI][TFSI] (red traces) (overall wt %) contents.

protic IL ensures narrower interfaces, thus facilitating ion transport and enhancing the overall performance.

The ionic conductivity of a PIMS PEM is determined by the number of dissociated ions, ionic mobility, and charge on the ionic species. The measured ionic conductivity of the PEMs increases more rapidly in comparison to the increment in the IL concentration (Figure 3). For example, the overall IL concentration in the PEM increases about 3.5-fold from PIMS-15 to PIMS-45, while the conductivity increases by a factor of ca. 12 at 100 °C. The observed increase in the conductivity is likely due to a combination of factors. The volume fraction of the IL in the conducting phase increases from 28% for PIMS-15 to 65% for PIMS-45, thus diluting the PEO chains and increasing the ionic mobility and intrinsic conductivity of the PEO/IL phase. Another important factor is the increase in the domain purity, a consequence of the increase in the segregation strength between the conducting PEO/IL and glassy PS domains with increasing IL content.[22] At low IL concentrations, a diffuse interface between the PS domains and conducting phase might increase the effective viscosity of the conducting channels. Overall, increasing the IL content increases the mobility and concentration of the ionic species while concurrently leading to a narrower interface between the insulating and conducting pathways.

Cross-Linked, Mechanically Robust Scaffold. "Ion gels" designed with ABA copolymers swollen with high IL contents exhibit excellent ionic conductivity.[60,64] However, increasing the polymer content to improve the modulus severely decreases

DOI: 10.1021/acsami.5b12366
ACS Appl. Mater. Interfaces 2016, 8, 6200−6210

the ionic conductivity of the system, and the lack of long-range continuity in the mechanically robust phase restricts these PEMs to moduli in the kilopascal range. In contrast to ABA triblock ion gels, diblock PEMs like PS-*b*-P2VP/IL with lamellar or cylindrical morphologies are capable of exhibiting decoupled mechanical and conducting characteristics owing to the higher extent of continuity present in both of the phases.[13,22] However, polymer electrolytes relying on glassy polymer backbones experience a sudden drop in the mechanical integrity above the glass transition temperature of the glassy polymer and even in the bulk diblock copolymers exhibit poor toughness.[21,64,70]

In the case of PIMS PEMs, we overcame these limitations by designing a PEM with a cocontinuous morphology and a chemically cross-linked robust insulating phase. Uniform growth of P(S-*co*-DVB) from PEO-CTA is critical to impart robustness to the system well above the glass transition temperature of linear PS ($T_g \approx 100$ °C). Long-range continuity of the cross-linked mechanical domain results in a robust, high-modulus PIMS-45 sample, even though more than half of the volume consists of the PEO/IL conducting phase. The absence of any loss of conductivity of high-IL-content membranes even at elevated temperatures underscores the high thermal stability of these PIMS PEMs. Consistent measurements of the ionic conductivity upon heating and cooling cycles further confirm the superior thermal response of the PEMs (Figure S5).

CONCLUSIONS

Mechanically robust and thermally stable polymer electrolyte membranes were synthesized by incorporating a protic IL into a cross-linked block polymer matrix. The simultaneous growth of the diblocks and cross-linking arrests the local segregation between the cross-linked PS phase and the conducting phase (PEO/IL), imparting a bicontinuous morphology to the nanostructured PEM. The long-range continuity of the conducting and mechanical phases allows the PIMS PEMs to achieve exceptional ionic conductivity without compromising the mechanical stability of the system, even at elevated temperatures. The measured PEM conductivity as a function of the IL concentration highlights the existence of isotropic continuous-conducting nanochannels even at low IL content. The high selectivity of the protic IL for the PEO phase leads to increased domain purity and narrower interfaces between the PEO/IL conducting domains and the rigid cross-linked PS phase, minimizing the diffusive resistance to ionic transport. In the absence of any proton donating groups on the polymer backbone, the proton-transport mechanism in the PEMs may be described as vehicular transport of the protons associated with the cations of the IL. PIMS PEMs incorporating protic ILs are very promising for high-temperature, anhydrous proton-transport applications. Further study in terms of developing membrane electrode assemblies and measuring current densities and fuel crossover rates will be necessary to establish the true potential of the PIMS PEMs as proton-exchange membranes for high-temperature fuel cells.

ASSOCIATED CONTENT

Supporting Information

The Supporting Information is available free of charge on the ACS Publications website at DOI: 10.1021/acsami.5b12366.

TGA weight loss analysis, DSC data, viscoelastic master curve, representative PFG-NMR data, and cation and anion diffusion coefficients in PIMS PEMs (PDF)

AUTHOR INFORMATION

Corresponding Authors

*E-mail: hillmyer@umn.edu.
*E-mail: lodge@umn.edu.

Notes

The authors declare no competing financial interest.

ACKNOWLEDGMENTS

This work was supported by the National Science Foundation (Grants DMR-1006370 and DMR-1206459). SAXS data were obtained at the APS, Sector 5 (DuPont−Northwestern−Dow Collaborative Access Team, DND-CAT) and Sector 12. DND-CAT is supported by The Dow Chemical Company, E. I. DuPont de Nemours & Co., and Northwestern University. Use of the APS, an Office of Science User Facility operated for the U.S. Department of Energy (DOE), Office of Science, by Argonne National Laboratory, was supported by the U.S. DOE under Contract DE-AC02-06CH11357. Portions of this work were carried out in the Characterization Facility, University of Minnesota, which receives partial support from the NSF through the MRSEC program (Grant DMR-1420013). The authors thank Prof. Philippe Bühlmann for access to his impedance spectroscopy equipment and Dr. Lucas McIntosh, Morgan Schulze, and Matthew Irwin for helpful discussions.

REFERENCES

(1) Armand, M.; Endres, F.; MacFarlane, D. R.; Ohno, H.; Scrosati, B. Ionic-Liquid Materials for the Electrochemical Challenges of the Future. *Nat. Mater.* **2009**, *8*, 621−629.
(2) Garcia, B.; Lavallée, S.; Perron, G.; Michot, C.; Armand, M. Room Temperature Molten Salts as Lithium Battery Electrolyte. *Electrochim. Acta* **2004**, *49*, 4583−4588.
(3) Seki, S.; Kobayashi, Y.; Miyashiro, H.; Ohno, Y.; Mita, Y.; Usami, A.; Terada, N.; Watanabe, M. Reversibility of Lithium Secondary Batteries Using a Room-Temperature Ionic Liquid Mixture and Lithium Metal. *Electrochem. Solid-State Lett.* **2005**, *8*, A577−A578.
(4) Doyle, M.; Choi, S. K.; Proulx, G. High-Temperature Proton Conducting Membranes Based on Perfluorinated Ionomer Membrane-Ionic Liquid Composites. *J. Electrochem. Soc.* **2000**, *147*, 34−37.
(5) Xu, W.; Angell, C. A. Solvent-Free Electrolytes with Aqueous Solution-like Conductivities. *Science* **2003**, *302*, 422−425.
(6) Belieres, J.-P.; Angell, C. A. Protic Ionic Liquids: Preparation, Characterization, and Proton Free Energy Level Representation. *J. Phys. Chem. B* **2007**, *111*, 4926−4937.
(7) Lee, S.-Y.; Yasuda, T.; Watanabe, M. Fabrication of Protic Ionic Liquid/sulfonated Polyimide Composite Membranes for Non-Humidified Fuel Cells. *J. Power Sources* **2010**, *195*, 5909−5914.
(8) Lee, J.; Panzer, M. J.; He, Y.; Lodge, T. P.; Frisbie, C. D. Ion Gel Gated Polymer Thin-Film Transistors. *J. Am. Chem. Soc.* **2007**, *129*, 4532−4533.
(9) Fernicola, A.; Panero, S.; Scrosati, B.; Tamada, M.; Ohno, H. New Types of Brönsted Acid-Base Ionic Liquids-Based Membranes for Applications in PEMFCs. *ChemPhysChem* **2007**, *8*, 1103−1107.
(10) Lee, S.-Y.; Ogawa, A.; Kanno, M.; Nakamoto, H.; Yasuda, T.; Watanabe, M. Nonhumidified Intermediate Temperature Fuel Cells Using Protic Ionic Liquids. *J. Am. Chem. Soc.* **2010**, *132*, 9764−9773.
(11) Young, W.-S.; Kuan, W.-F.; Epps, T. H. Block Copolymer Electrolytes for Rechargeable Lithium Batteries. *J. Polym. Sci., Part B: Polym. Phys.* **2014**, *52*, 1−16.

(12) Singh, B.; Sekhon, S. S. Ion Conducting Behaviour of Polymer Electrolytes Containing Ionic Liquids. *Chem. Phys. Lett.* **2005**, *414*, 34−39.
(13) Gwee, L.; Choi, J.-H.; Winey, K. I.; Elabd, Y. A. Block Copolymer/Ionic Liquid Films: The Effect of Ionic Liquid Composition on Morphology and Ion Conduction. *Polymer* **2010**, *51*, 5516−5524.
(14) Kim, S. Y.; Yoon, E.; Joo, T.; Park, M. J. Morphology and Conductivity in Ionic Liquid Incorporated Sulfonated Block Copolymers. *Macromolecules* **2011**, *44*, 5289−5298.
(15) Miranda, D. F.; Russell, T. P.; Watkins, J. J. Ordering in Mixtures of a Triblock Copolymer with a Room Temperature Ionic Liquid. *Macromolecules* **2010**, *43*, 10528−10535.
(16) Simone, P. M.; Lodge, T. P. Phase Behavior and Ionic Conductivity of Concentrated Solutions of Polystyrene-Poly(ethylene oxide) Diblock Copolymers in an Ionic Liquid. *ACS Appl. Mater. Interfaces* **2009**, *1*, 2812−2820.
(17) Virgili, J. M.; Hexemer, A.; Pople, J. A.; Balsara, N. P.; Segalman, R. A. Phase Behavior of Polystyrene-*block*-poly(2-vinylpyridine) Copolymers in a Selective Ionic Liquid Solvent. *Macromolecules* **2009**, *42*, 4604−4613.
(18) Wanakule, N. S.; Virgili, J. M.; Teran, A. A.; Wang, Z.-G.; Balsara, N. P. Thermodynamic Properties of Block Copolymer Electrolytes Containing Imidazolium and Lithium Salts. *Macromolecules* **2010**, *43*, 8282−8289.
(19) Young, W.-S.; Epps, T. H. Ionic Conductivities of Block Copolymer Electrolytes with Various Conducting Pathways: Sample Preparation and Processing Considerations. *Macromolecules* **2012**, *45*, 4689−4697.
(20) Kim, S. Y.; Lee, J.; Park, M. J. Proton Hopping and Diffusion Behavior of Sulfonated Block Copolymers Containing Ionic Liquids. *Macromolecules* **2014**, *47*, 1099−1108.
(21) Kim, S. Y.; Kim, S.; Park, M. J. Enhanced Proton Transport in Nanostructured Polymer Electrolyte/ionic Liquid Membranes under Water-Free Conditions. *Nat. Commun.* **2010**, *1*, 1−7.
(22) Hoarfrost, M. L.; Segalman, R. A. Ionic Conductivity of Nanostructured Block Copolymer/Ionic Liquid Membranes. *Macromolecules* **2011**, *44*, 5281−5288.
(23) Wilkes, J. S. A Short History of Ionic Liquids—from Molten Salts to Neoteric Solvents. *Green Chem.* **2002**, *4*, 73−80.
(24) Sangoro, J. R.; Serghei, A.; Naumov, S.; Galvosas, P.; Kärger, J.; Wespe, C.; Bordusa, F.; Kremer, F. Charge Transport and Mass Transport in Imidazolium-Based Ionic Liquids. *Phys. Rev. E: Stat., Nonlinear, Soft Matter Phys.* **2008**, *77*, 051202.
(25) Green, M. D.; Long, T. E. Designing Imidazole-Based Ionic Liquids and Ionic Liquid Monomers for Emerging Technologies. *Polym. Rev.* **2009**, *49*, 291−314.
(26) Welton, T. Room-Temperature Ionic Liquids. Solvents for Synthesis and Catalysis. *Chem. Rev.* **1999**, *99*, 2071−2084.
(27) Ohno, H.; Yoshizawa, M. Ion Conductive Characteristics of Ionic Liquids Prepared by Neutralization of Alkylimidazoles. *Solid State Ionics* **2002**, *154-155*, 303−309.
(28) Noda, A.; Susan, M. A. B. H.; Kudo, K.; Mitsushima, S.; Hayamizu, K.; Watanabe, M. Brønsted Acid - Base Ionic Liquids as Proton-Conducting Nonaqueous Electrolytes. *J. Phys. Chem. B* **2003**, *107*, 4024−4033.
(29) Hoarfrost, M. L.; Tyagi, M.; Segalman, R. A.; Reimer, J. A. Proton Hopping and Long-Range Transport in the Protic Ionic Liquid [Im][TFSI], Probed by Pulsed-Field Gradient NMR and Quasi-Elastic Neutron Scattering. *J. Phys. Chem. B* **2012**, *116*, 8201−8209.
(30) Susan, M. A. B. H.; Noda, A.; Mitsushima, S.; Watanabe, M. Brønsted Acid-Base Ionic Liquids and Their Use as New Materials for Anhydrous Proton Conductors. *Chem. Commun.* **2003**, *8*, 938−939.
(31) Yasuda, T.; Watanabe, M. Protic Ionic Liquids: Fuel Cell Applications. *MRS Bull.* **2013**, *38*, 560−566.
(32) Nakamoto, H.; Watanabe, M. Brønsted Acid-Base Ionic Liquids for Fuel Cell Electrolytes. *Chem. Commun.* **2007**, *24*, 2539−2541.
(33) Yan, F.; Yu, S.; Zhang, X.; Qiu, L.; Chu, F.; You, J.; Lu, J. Enhanced Proton Conduction in Polymer Electrolyte Membranes as Synthesized by Polymerization of Protic Ionic Liquid-Based Microemulsions. *Chem. Mater.* **2009**, *21*, 1480−1484.
(34) Tang, Q.; Wu, J.; Tang, Z.; Li, Y.; Lin, J. High-Temperature Proton Exchange Membranes from Ionic Liquid Absorbed/doped Superabsorbents. *J. Mater. Chem.* **2012**, *22*, 15836−15844.
(35) Hallinan, D. T.; Balsara, N. P. Polymer Electrolytes. *Annu. Rev. Mater. Res.* **2013**, *43*, 503−525.
(36) Weber, R. L.; Ye, Y.; Schmitt, A. L.; Banik, S. M.; Elabd, Y. A.; Mahanthappa, M. K. Effect of Nanoscale Morphology on the Conductivity of Polymerized Ionic Liquid Block Copolymers. *Macromolecules* **2011**, *44*, 5727−5735.
(37) Zawodzinski, T. A. Water Uptake by and Transport Through Nafion® 117 Membranes. *J. Electrochem. Soc.* **1993**, *140*, 1041−1047.
(38) Hoarfrost, M. L.; Tyagi, M. S.; Segalman, R. A.; Reimer, J. A. Effect of Confinement on Proton Transport Mechanisms in Block Copolymer/ionic Liquid Membranes. *Macromolecules* **2012**, *45*, 3112−3120.
(39) Wu, W.; Li, Y.; Chen, P.; Liu, J.; Wang, J.; Zhang, H. Constructing Ionic Liquid-Filled Proton Transfer Channels within Nanocomposite Membrane by Using Functionalized Graphene Oxide. *ACS Appl. Mater. Interfaces* **2016**, *8*, 588−599.
(40) Weber, R. L.; Ye, Y.; Banik, S. M.; Elabd, Y. A.; Hickner, M. A.; Mahanthappa, M. K. Thermal and Ion Transport Properties of Hydrophilic and Hydrophobic Polymerized Styrenic Imidazolium Ionic Liquids. *J. Polym. Sci., Part B: Polym. Phys.* **2011**, *49*, 1287−1296.
(41) Park, M. J.; Balsara, N. P. Anisotropic Proton Conduction in Aligned Block Copolymer Electrolyte Membranes at Equilibrium with Humid Air. *Macromolecules* **2010**, *43*, 292−298.
(42) Bates, F. S. Network Phases in Block Copolymer Melts. *MRS Bull.* **2005**, *30*, 525−532.
(43) Schulze, M. W.; McIntosh, L. D.; Hillmyer, M. A.; Lodge, T. P. High-Modulus, High-Conductivity Nanostructured Polymer Electrolyte Membranes via Polymerization-Induced Phase Separation. *Nano Lett.* **2014**, *14*, 122−126.
(44) Walker, C. N.; Bryson, K. C.; Hayward, R. C.; Tew, G. N. Wide Bicontinuous Compositional Windows from Co-Networks Made with Telechelic Macromonomers. *ACS Nano* **2014**, *8*, 12376−12385.
(45) Price, S. C.; Ren, X.; Jackson, A. C.; Ye, Y.; Elabd, Y. A.; Beyer, F. L. Bicontinuous Alkaline Fuel Cell Membranes from Strongly Self-Segregating Block Copolymers. *Macromolecules* **2013**, *46*, 7332−7340.
(46) McIntosh, L. D.; Schulze, M. W.; Irwin, M. T.; Hillmyer, M. A.; Lodge, T. P. Evolution of Morphology, Modulus, and Conductivity in Polymer Electrolytes Prepared via Polymerization-Induced Phase Separation. *Macromolecules* **2015**, *48*, 1418−1428.
(47) Lee, S.; Gillard, T. M.; Bates, F. S. Fluctuations, Order, and Disorder in Short Diblock Copolymers. *AIChE J.* **2013**, *59*, 3502−3513.
(48) Lai, J. T.; Filla, D.; Shea, R. Functional Polymers from Novel Carboxyl-Terminated Trithiocarbonates as Highly Efficient RAFT Agents. *Macromolecules* **2002**, *35*, 6754−6756.
(49) Mao, H.; Hillmyer, M. A. Nanoporous Polystyrene by Chemical Etching of Poly(ethylene oxide) from Ordered Block Copolymers. *Macromolecules* **2005**, *38*, 4038−4039.
(50) Wu, D.; Chen, A.; Johnson, C. S. An Improved Diffusion Ordered Spectroscopy Experiment Incorporating Bipolar Gradient Pulses. *J. Magn. Reson., Ser. A* **1995**, *115*, 260−264.
(51) Seo, M.; Hillmyer, M. A. Reticulated Nanoporous Polymers by Controlled Polymerization-Induced Microphase Separation. *Science* **2012**, *336*, 1422−1425.
(52) Lodge, T. P.; Pudil, B.; Hanley, K. J. The Full Phase Behavior for Block Copolymers in Solvents of Varying Selectivity. *Macromolecules* **2002**, *35*, 4707−4717.
(53) Young, W.-S.; Epps, T. H. Salt Doping in PEO-Containing Block Copolymers: Counterion and Concentration Effects. *Macromolecules* **2009**, *42*, 2672−2678.
(54) Hoarfrost, M. L.; Segalman, R. A. Conductivity Scaling Relationships for Nanostructured Block copolymer/Ionic Liquid Membranes. *ACS Macro Lett.* **2012**, *1*, 937−943.

DOI: 10.1021/acsami.5b12366
ACS Appl. Mater. Interfaces 2016, 8, 6200−6210

(55) Milhaupt, J. M.; Lodge, T. P. Homopolymer and Small-molecule Tracer Diffusion in a Gyroid Matrix. *J. Polym. Sci., Part B: Polym. Phys.* **2001**, *39*, 843−859.
(56) Phillip, W. A.; Amendt, M.; O'Neill, B.; Chen, L.; Hillmyer, M. A.; Cussler, E. L. Diffusion and Flow across Nanoporous Polydicyclopentadiene-Based Membranes. *ACS Appl. Mater. Interfaces* **2009**, *1*, 472−480.
(57) Chen, L.; Phillip, W. A.; Cussler, E. L.; Hillmyer, M. A. Robust Nanoporous Membranes Templated by a Doubly Reactive Block Copolymer. *J. Am. Chem. Soc.* **2007**, *129*, 13786−13787.
(58) Rey, I.; Johansson, P.; Lindgren, J.; Lassègues, J. C.; Grondin, J.; Servant, L. Spectroscopic and Theoretical Study of $(CF_3SO_2)_2N^-$ ($TFSI^-$) and $(CF_3SO_2)_2NH$ (HTFSI). *J. Phys. Chem. A* **1998**, *102*, 3249−3258.
(59) Noda, A.; Hayamizu, K.; Watanabe, M. Pulsed-Gradient Spin - Echo ^1H and ^{19}F NMR Ionic Diffusion Coefficient, Viscosity, and Ionic Conductivity of Non-Chloroaluminate Room-Temperature Ionic Liquids. *J. Phys. Chem. B* **2001**, *105*, 4603−4610.
(60) Zhang, S.; Lee, K. H.; Sun, J.; Frisbie, C. D.; Lodge, T. P. Viscoelastic Properties, Ionic Conductivity, and Materials Design Considerations for Poly(styrene-*b*-ethylene oxide-*b*-styrene)-Based Ion Gel Electrolytes. *Macromolecules* **2011**, *44*, 8981−8989.
(61) Singh, M.; Odusanya, O.; Wilmes, G. M.; Eitouni, H. B.; Gomez, E. D.; Patel, A. J.; Chen, V. L.; Park, M. J.; Fragouli, P.; Iatrou, H.; Hadjichristidis, N.; Cookson, D.; Balsara, N. P. Effect of Molecular Weight on the Mechanical and Electrical Properties of Block Copolymer Electrolytes. *Macromolecules* **2007**, *40*, 4578−4585.
(62) Li, Q.; He, R.; Jensen, J. O.; Bjerrum, N. J. Approaches and Recent Development of Polymer Electrolyte Membranes for Fuel Cells Operating above 100 °C. *Chem. Mater.* **2003**, *15*, 4896−4915.
(63) Jones, G.; McGhie, A.; Farrington, G. Studies of the Stability of Poly (ethylene oxide) and PEO-Based Solid Electrolytes Using Thermogravimetry-Mass Spectrometry. *Macromolecules* **1991**, *24*, 3285−3290.
(64) Zhang, S.; Lee, K. H.; Frisbie, C. D.; Lodge, T. P. Ionic Conductivity, Capacitance, and Viscoelastic Properties of Block Copolymer-Based Ion Gels. *Macromolecules* **2011**, *44*, 940−949.
(65) Kim, O.; Jo, G.; Park, Y. J.; Kim, S.; Park, M. J. Ion Transport Properties of Self-Assembled Polymer Electrolytes: The Role of Confinement and Interface. *J. Phys. Chem. Lett.* **2013**, *4*, 2111−2117.
(66) Gido, S. P.; Thomas, E. L. Lamellar Diblock Copolymer Grain Boundary Morphology. 4. Tilt Boundaries. *Macromolecules* **1994**, *27*, 6137−6144.
(67) Zhang, H.; Wu, W.; Wang, J.; Zhang, T.; Shi, B.; Liu, J.; Cao, S. Enhanced Anhydrous Proton Conductivity of Polymer Electrolyte Membrane Enabled by Facile Ionic Liquid-Based Hoping Pathways. *J. Membr. Sci.* **2015**, *476*, 136−147.
(68) Freire, M. G.; Santos, L. M. N. B. F.; Fernandes, A. M.; Coutinho, J. A. P.; Marrucho, I. M. An Overview of the Mutual Solubilities of Water−imidazolium-Based Ionic Liquids Systems. *Fluid Phase Equilib.* **2007**, *261*, 449−454.
(69) Simone, P. M.; Lodge, T. P. Lyotropic Phase Behavior of Polybutadiene−Poly(ethylene oxide) Diblock Copolymers in Ionic Liquids. *Macromolecules* **2008**, *41*, 1753−1759.
(70) Susan, M. A. B. H.; Kaneko, T.; Noda, A.; Watanabe, M. Ion Gels Prepared by in Situ Radical Polymerization of Vinyl Monomers in an Ionic Liquid and Their Characterization as Polymer Electrolytes. *J. Am. Chem. Soc.* **2005**, *127*, 4976−4983.

DOI: 10.1021/acsami.5b12366
ACS Appl. Mater. Interfaces 2016, 8, 6200−6210